Cryogen-free heterodyne-enhanced mid-infrared Faraday rotation spectrometer

Yin Wang, Michal Nikodem, and Gerard Wysocki*

Electrical Engineering Department, Princeton University, Princeton, New Jersey, 08544, USA
gwysocki@princeton.edu

Abstract: A new detection method for Faraday rotation spectra of paramagnetic molecular species is presented. Near shot-noise limited performance in the mid-infrared is demonstrated using a heterodyne enhanced Faraday rotation spectroscopy (H-FRS) system without any cryogenic cooling. Theoretical analysis is performed to estimate the ultimate sensitivity to polarization rotation for both heterodyne and conventional FRS. Sensing of nitric oxide (NO) has been performed with an H-FRS system based on thermoelectrically cooled 5.24 μm quantum cascade laser (QCL) and a mercury-cadmium-telluride photodetector. The QCL relative intensity noise that dominates at low frequencies is largely avoided by performing the heterodyne detection in radio frequency range. H-FRS exhibits a total noise level of only 3.7 times the fundamental shot noise. The achieved sensitivity to polarization rotation of 1.8×10^{-8} rad/Hz$^{1/2}$ is only 5.6 times higher than the ultimate theoretical sensitivity limit estimated for this system. The path- and bandwidth-normalized NO detection limit of 3.1 ppbv-m/Hz$^{1/2}$ was achieved using the R(17/2) transition of NO at 1906.73 cm^{-1}.

OCIS codes: (300.6390) Spectroscopy, molecular; (300.6310) Spectroscopy, heterodyne; (140.5965) Semiconductor lasers, quantum cascade.

References and links

1. G. Litfin, C. R. Pollock, R. F. Curl, and F. K. Tittel, "Sensitivity Enhancement of Laser-Absorption Spectroscopy by Magnetic Rotation Effect," J. Chem. Phys. **72**(12), 6602–6605 (1980).
2. H. Adams, D. Reinert, P. Kalkert, and W. Urban, "A differential detection scheme for Faraday rotation spectroscopy with a color center laser," Appl. Phys. B **34**(4), 179–185 (1984).
3. M. Koch, X. Luo, P. Murtz, W. Urban, and K. Morike, "Detection of small traces of $^{15}N_2$ and $^{15}N_2$ by Faraday LMR spectroscopy of the corresponding isotopomers of nitric oxide," Appl. Phys. B **64**(6), 683–688 (1997).
4. H. Ganser, W. Urban, and A. M. Brown, "The sensitive detection of NO by Faraday modulation spectroscopy with a quantum cascade laser," Mol. Phys. **101**(4-5), 545–550 (2003).
5. T. Fritsch, M. Horstjann, D. Halmer, P. Sabana, P. Hering, and M. Mürtz, "Magnetic Faraday modulation spectroscopy of the 1-0 band of ^{14}NO and ^{15}NO," Appl. Phys. B **93**(2-3), 713–723 (2008).
6. R. Lewicki, J. H. Doty 3rd, R. F. Curl, F. K. Tittel, and G. Wysocki, "Ultrasensitive detection of nitric oxide at 5.33 microm by using external cavity quantum cascade laser-based Faraday rotation spectroscopy," Proc. Natl. Acad. Sci. U.S.A. **106**(31), 12587–12592 (2009).
7. P. Kluczynski, S. Lundqvist, J. Westberg, and O. Axner, "Faraday rotation spectrometer with sub-second response time for detection of nitric oxide using a cw DFB quantum cascade laser at 5.33 μm," Appl. Phys. B **103**(2), 451–459 (2011).
8. J. M. Smith, J. C. Bloch, R. W. Field, and J. L. Steinfeld, "Trace Detection of NO_2 by Frequency-Modulation-Enhanced Magnetic Rotation Spectroscopy," J. Opt. Soc. Am. B **12**(6), 964–969 (1995).
9. W. Dillenschneider and R. F. Curl, Jr., "Color center laser spectroscopy of v1 + v2 + v3 of NO_2 using magnetic rotation," J. Mol. Spectrosc. **99**(1), 87–97 (1983).
10. R. J. Brecha, L. M. Pedrotti, and D. Krause, "Magnetic rotation spectroscopy of molecular oxygen with a diode laser," J. Opt. Soc. Am. B **14**(8), 1921–1930 (1997).
11. S. G. So, E. Jeng, and G. Wysocki, "VCSEL based Faraday rotation spectroscopy with a modulated and static magnetic field for trace molecular oxygen detection," Appl. Phys. B **102**(2), 279–291 (2011).
12. J. Pfeiffer, D. Kirsten, P. Kalkert, and W. Urban, "Sensitive Magnetic Rotation Spectroscopy of the Oh Free-Radical Fundamental-Band with a Color Center Laser," Appl. Phys. B **26**(3), 173–177 (1981).

#177574 - $15.00 USD Received 8 Oct 2012; revised 20 Nov 2012; accepted 21 Dec 2012; published 7 Jan 2013

13. W. Zhao, G. Wysocki, W. Chen, E. Fertein, D. Le Coq, D. Petitprez, and W. Zhang, "Sensitive and selective detection of OH radicals using Faraday rotation spectroscopy at 2.8 μm," Opt. Express **19**(3), 2493–2501 (2011).
14. M. Nikodem and G. Wysocki, "Molecular dispersion spectroscopy--new capabilities in laser chemical sensing," Ann. N. Y. Acad. Sci. **1260**(1), 101–111 (2012).
15. A. Hinz, D. Zeitz, W. Bohle, and W. Urban, "A Faraday Laser Magnetic-Resonance Spectrometer for Spectroscopy of Molecular Radical Ions," Appl. Phys. B **36**(1), 1–4 (1985).
16. H. Adams, D. Reinert, P. Kalkert, and W. Urban, "A Differential Detection Scheme for Faraday-Rotation Spectroscopy with a Color Center Laser," Appl. Phys. B. **34**(4), 179–185 (1984).
17. R. Engeln, G. Berden, R. Peeters, and G. Meijer, "Cavity enhanced absorption and cavity enhanced magnetic rotation spectroscopy," Rev. Sci. Instrum. **69**(11), 3763–3769 (1998).
18. P. C. D. Hobbs, "Shot noise limited optical measurement at baseband with noisy lasers," in *Laser Noise*, R. Roy, ed. (Proc. SPIE, 1991), pp. 216–221.
19. K. L. Haller and P. C. D. Hobbs, "Double-beam laser absorption spectroscopy: shot noise-limited performance at baseband with a novel electronic noise canceler," in *Optical Methods for Ultrasensitive Detection and Analysis: Techniques and Applications,*(1991), pp. 298–309.
20. G. Durry, I. Pouchet, N. Amarouche, T. Danguy, and G. Megie, "Shot-noise-limited dual-beam detector for atmospheric trace-gas monitoring with near-infrared diode lasers," Appl. Opt. **39**(30), 5609–5619 (2000).
21. X. Wang, M. Jefferson, P. C. D. Hobbs, W. P. Risk, B. E. Feller, R. D. Miller, and A. Knoesen, "Shot-noise limited detection for surface plasmon sensing," Opt. Express **19**(1), 107–117 (2011).
22. P. Vogel and V. Ebert, "Near shot noise detection of oxygen in the A-band with vertical-cavity surface-emitting lasers," Appl. Phys. B **72**(1), 127–135 (2001).
23. N. C. Wong and J. L. Hall, "Servo control of amplitude-modulation in frequency-modulation spectroscopy - demonstration of shot-noise-limited detection," J. Opt. Soc. Am. B **2**(9), 1527–1533 (1985).
24. B. Willke, N. Uehara, E. K. Gustafson, R. L. Byer, P. J. King, S. U. Seel, and R. L. Savage, Jr., "Spatial and temporal filtering of a 10-W Nd:YAG laser with a Fabry--Perot ring-cavity premode cleaner," Opt. Lett. **23**(21), 1704–1706 (1998).
25. P. Kwee, B. Willke, and K. Danzmann, "Shot-noise-limited laser power stabilization with a high-power photodiode array," Opt. Lett. **34**(19), 2912–2914 (2009).
26. M. Jurna, J. P. Korterik, C. Otto, and H. L. Offerhaus, "Shot noise limited heterodyne detection of CARS signals," Opt. Express **15**(23), 15207–15213 (2007).
27. M. C. Teich, "Infrared heterodyne detection," Proc. IEEE **56**(1), 37–46 (1968).
28. S. F. Jacobs, "Optical heterodyne (coherent) detection," Am. J. Phys. **56**(3), 235–245 (1988).
29. E. N. Gilbert, and H. O. Pollak, "Amplitude Distribution of Shot Noise," AT&T Tech J **39**, 333–350 (1960).
30. M. Xiao, L. A. Wu, and H. J. Kimble, "Precision measurement beyond the shot-noise limit," Phys. Rev. Lett. **59**(3), 278–281 (1987).
31. T. Gensty, W. Elsäßer, and C. Mann, "Intensity noise properties of quantum cascade lasers," Opt. Express **13**(6), 2032–2039 (2005).
32. F. Rana and R. J. Ram, "Current noise and photon noise in quantum cascade lasers," Phys. Rev. B **65**(12), 125313 (2002).
33. Y. Wang, M. Nikodem, J. Hoyne, and G. Wysocki, "Heterodyne-enhanced Faraday rotation spectrometer," Proc. SPIE 8268, 2F1–8 (2012).
34. A. Abramovici, W. E. Althouse, R. W. P. Drever, Y. Gürsel, S. Kawamura, F. J. Raab, D. Shoemaker, L. Sievers, R. E. Spero, K. S. Thorne, R. E. Vogt, R. Weiss, S. E. Whitcomb, and M. E. Zucker, "LIGO - the Laser-Interferometer-Gravitational-Wave-Observatory," Science **256**(5055), 325–333 (1992).
35. Y. Wang, M. Nikodem, B. Brumfield, and G. Wysocki, "Compact multi-pass cell based Faraday rotation spectrometer for nitric oxide detection," in *Conference on Lasers and Electro-Optics (CLEO)*(2012), p. CW3B.
36. E. J. Galvez and P. M. Koch, "Use of four mirrors to rotate linear polarization but preserve input-output collinearity. II," J. Opt. Soc. Am. A **14**(12), 3410–3414 (1997).
37. C. D. Boone, F. W. Dalby, and I. Ozier, "Magnetic rotation molecular spectroscopy using an oscillating field," J. Chem. Phys. **113**(19), 8594–8607 (2000).

1. Introduction

Since first reported in the 1980s [1], Faraday rotation spectroscopy (FRS) has been used as a sensitive and selective technique for the detection of gas-phase paramagnetic species such as NO [1–7], NO_2 [8, 9], O_2 [10, 11], and OH radicals [12, 13]. In the presence of magnetic field, the transition states of the paramagnetic molecules split due to the Zeeman Effect causing magnetic circular birefringence (MCB, a difference in refractive indices for left-handed (LHCP), and right-handed (RHCP) circularly polarized components) and magnetic circular dichroism (MCD, a difference in absorption coefficients for LHCP and RHCP). When linearly polarized light, which is a superposition of LHCP and RHCP, propagates in the paramagnetic sample under longitudinal magnetic field, it exhibits rotation of the polarization axis (the Faraday Effect). At low concentrations of the target molecules the absorption is

#177574 - $15.00 USD Received 8 Oct 2012; revised 20 Nov 2012; accepted 21 Dec 2012; published 7 Jan 2013

small and the MCD is usually negligible. The polarization rotation angle can be described as $\Theta = (n_R - n_L)\pi L/\lambda$, where L is the effective optical path length within the sample under magnetic field, λ is the wavelength of light and $(n_R - n_L)$ is a difference between refractive indices for RHCP and LHCP components. Since Faraday rotation Θ is proportional to sample concentration it can be used for quantitative measurements of sample concentration.

Typically to perform FRS measurements a polarizer is placed before the sample to establish a well-defined polarization state of the incident light and a nearly crossed polarizer (analyzer) is placed after the sample to convert the polarization rotation to light intensity changes (this arrangement is referred to as "90-degree method"). The light intensity is then detected with a photodetector. This nearly crossed analyzer is very effective in suppression of the laser intensity noise, which improves the signal-to-noise ratio (SNR) of an FRS system. Further suppression of broadband noise is usually performed through reduction of the measurement bandwidth achieved with modulated magnetic field and phase sensitive lock-in detection. Typically the FRS is able to provide several orders of magnitude more sensitive molecular detection than equivalent direct absorption spectroscopy systems [1, 6, 14].

The most common practices reported to-date in the literature to improve FRS system performance were mostly focused on increase in the FRS signal strength, and on optimization of the analyzer offset angle θ. Several strategies focused on the FRS signal increase have been reported including: selection of molecular transitions with higher intensity [4–7, 13], providing optimal magnetic field strength [5, 7, 10], optimizing the sample pressures [5, 10, 11], using higher laser power or minimizing the losses in the gas cell [7], increasing the optical path with multi-pass cells [15, 16], as well as applying cavity enhanced techniques [17]. Since analyzer offset angle θ (measured from the crossed position) affects both the signal strength as well as the total noise received by the photodetector, optimization of θ must be performed for each FRS system individually. The total noise measured in FRS system is composed of photodetector noise, laser intensity noise, and shot noise. The latter two are related to the intensity of laser light on the photodetector and thus depend on θ (through the Malus Law the laser noise is proportional to $\sin^2(\theta)$ and the shot noise is proportional to $\sin(\theta)$), while the photodetector noise is θ-independent. Once sample properties and all system parameters are known (such as laser power, relative intensity noise (RIN), optical losses, magnetic field strength, effective optical path etc.) the system's SNR depends only on the analyzer offset angle θ. Its optimum value is chosen so that contribution from laser intensity noise matches the photodetector noise [1, 5–7, 11, 13]. For low RIN laser sources a decrease in θ might result in the shot noise becoming larger than the laser noise, which is a desired regime of operation that provides the ultimate system sensitivity. Since majority of mid-infrared (mid-IR) FRS instruments reported to date [5–7] showed significant domination of laser noise over the shot noise, one can conclude that in order to further enhance sensitivity of the mid-IR FRS systems, suppression of the laser RIN or decrease in the photodetector noise (that allows for decrease in θ) are the best strategies to approach the ultimate shot-noise limited performance.

The photodetector noise can be reduced by selecting an appropriate detector element with a low-noise pre-amplifier. The performance of mid-IR detectors is often significantly improved through cryogenic cooling of the detector element, which helps reducing the thermal noise that dominates in this spectral range. However this approach represents a logistical challenge and cryogen-free detectors are preferred in sensor systems intended for autonomous long-term measurements especially in field settings. Therefore in this work we focus on reduction of the laser noise, which is challenging, but can significantly improve performance of FRS systems and provide more relaxed requirements for low-noise photodetectors.

In general many spectroscopic systems are limited by laser noise, and the most popular techniques used to suppress the laser noise include: a) balanced detection incorporated with electronic noise canceller [18–22], b) active laser intensity stabilization [23–25], and c)

#177574 - $15.00 USD Received 8 Oct 2012; revised 20 Nov 2012; accepted 21 Dec 2012; published 7 Jan 2013

heterodyne detection [26–28]. All these techniques have been successful in avoiding or suppressing the excess laser noise in spectroscopic systems to the degree that the shot noise becomes dominant.

Shot noise arises from the intrinsic quantum nature of the photogenerated detector current and is usually the ultimate sensitivity limitation of optical detection systems (except for some special techniques involving amplitude-squeezed light sources that allow measurements beyond the shot-noise limit) [29, 30]. This fundamental limit represents the minimum detectable fluctuation of the field at the level of $1/N^{1/2}$, where N is a mean photoelectron number generated by the photodetector. As recently demonstrated by Zhao *et al.*, when very low optical power (at μW level) is used in combination with a sensitive thermoelectrically cooled (TEC) mercury cadmium telluride (MCT) photodetector, a shot-noise-dominated FRS of OH radicals at ~2.8 μm could be realized [13]. However up to now, no cryogen-free FRS system has been able to approach the fundamental limit in the mid-IR spectral range at wavelengths >3μm. For quantum cascade lasers (QCLs), that are currently very popular spectroscopic laser sources in the mid-IR, the main limitation is their intrinsic RIN that is relatively high. Due to their specific cascaded quantum-well structure and electron transport, the QCLs exhibit higher RIN than for example inter-band diode lasers [31, 32]. Additionally amplitude squeezing is difficult in QCLs, which makes sub-shot-noise limited detection significantly more challenging [32].

All three RIN suppression methods mentioned above have a chance to reduce the QCL noise and ultimately improve the FRS performance. For example, QCL RIN can be effectively suppressed using FRS with a balanced detection scheme (referred to as "45-degree FRS method", because the analyzer is set at 45° with respect to the incident polarization plane to give access to two polarization components with equal intensities used for balanced FRS measurement) [16]. Although very elegant, this approach is difficult to realize in mid-IR, because specialized dual element photodetectors with balanced differential preamplifiers are not readily available and costly if custom made. To mitigate the need for specialized detectors, in this work we present a new heterodyne enhanced FRS (H-FRS) technique that provides significant noise reduction by employing heterodyne detection of the FRS signal. H-FRS effectively shifts the FRS signal detection to radio frequency (RF) range where the QCL RIN is significantly lower. The developed system is cryogen-free and is based on a distributed feedback (DFB) QCL and a single MCT photodetector, both thermoelectrically cooled. The sensitivity to the polarization rotation was improved by almost two orders of magnitude as compared to the previous conventional FRS (C-FRS) system for NO detection reported in Ref [6]. and by one order of magnitude as compared to the work by Zhao *et al*. [13]. In section 2, a theoretical analysis of H-FRS is provided followed by the description of experimental setup in section 3 and noise characterization, performance tests of the prototype H-FRS system and discussion of the results presented in section 4.

2. Theoretical model for the signal and noise in H-FRS

A detailed theoretical modeling of the conventional FRS based on Jones matrices is provided in [33]. In this section, the SNR in H-FRS is analyzed and compared to the theoretical SNR of C-FRS systems. The condition for shot noise limited performance and ultimate achievable polarization rotation sensitivity are derived as well.

2.1. H-FRS operation principle

In the conventional FRS the detection limit can be expressed as a noise-equivalent Faraday rotation angle (Θ_{NEA}), a figure of merit that can be conveniently used to compare the results from different FRS systems. For a laser/detector noise dominated system with an assumption that at the optimum analyzer offset angle θ the laser noise and the detector noise are equal the noise-equivalent Faraday rotation angle becomes [33]:

#177574 - $15.00 USD Received 8 Oct 2012; revised 20 Nov 2012; accepted 21 Dec 2012; published 7 Jan 2013

$$\Theta_{NEA_{C-FRS}} = \sqrt{\frac{\Delta f \cdot NEP(\omega_m) \cdot \sigma(\omega_m)}{2P_0}} \quad (1)$$

where P_0 is the laser power before the polarization analyzer, Δf is the detection bandwidth (set by the lock-in amplifier), NEP(ω_m) and $\sigma(\omega_m)$ are the photodetector noise equivalent power and RIN of the laser source measured at the modulation frequency ω_m (frequency of the magnetic field modulation), respectively. Equation (1) was derived with an assumption that the laser noise contribution due to optical power leakage through a non-ideal polarizer is negligible, which is a reasonable assumption for polarizers with extinction ratio of 10^{-5} used in this work.

Since the modulation frequency ω_m in the C-FRS is rather low (<10 kHz), the sensitivity is typically limited by the excess RIN of the laser source at baseband. By implementing an optical heterodyne detection that shifts the FRS signal to high frequencies away from the baseband the sensitivity of the FRS system can be significantly improved and can approach the fundamental shot noise limit. In this work Θ_{NEA} will be used to gauge the performance of the H-FRS against other C-FRS systems reported in the literature.

In the H-FRS, by superimposing a local oscillator (LO) field with the FRS signal field emerging from the analyzer, a heterodyne beatnote can be created at frequency that is far above the noisy baseband region. The simplest way to create the LO is to recycle the extraordinary beam emerging from the analyzer that is polarized orthogonally with respect to the signal polarization. This beam contains most of the laser power that is usually lost in a conventional FRS system. In H-FRS a Rochon prism or any other high quality polarizer that gives access to both polarization components simultaneously (i.e. Wollaston prism) can be used as an analyzer as shown in Fig. 1(a). An optical frequency shifter (e.g. acousto-optical modulator, AOM) is used to create LO wave that is shifted by a well-defined RF frequency with respect to the signal wave. By recombining the signal beam and the LO beam on a beam splitter a heterodyne Mach-Zender interferometer is formed.

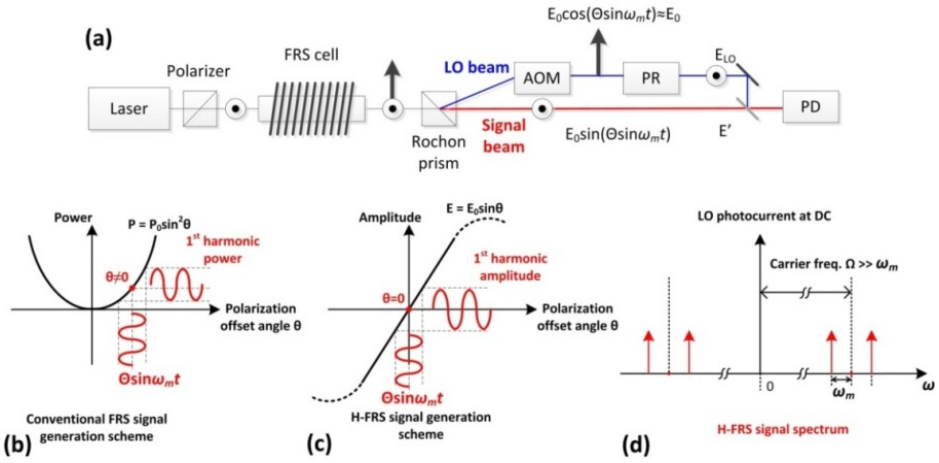

Fig. 1. (a) A concept diagram for the H-FRS system configuration. The extraordinary beam exiting the Rochon prism is frequency-shifted by AOM, and serves as the LO wave. Since its polarization is orthogonal to the signal wave, a polarization rotator (PR) was used to transform its polarization axis by 90° and assure maximum heterodyne efficiency. A principle of signal generation is schematically shown for conventional FRS in (b) and for H-FRS in (c). (d) An electrical RF spectrum of the photocurrent in H-FRS is an equivalent of a carrier-suppressed amplitude modulated signal.

In C-FRS, the photodetector collects the light transmitted through an analyzer, thus the intensity on the photodetector is proportional to $\sin^2\theta + \xi$ (ξ is the polarizer extinction ratio,

#177574 - $15.00 USD Received 8 Oct 2012; revised 20 Nov 2012; accepted 21 Dec 2012; published 7 Jan 2013

which usually is in 10^{-4}-10^{-5} range and can be neglected for $\theta > 0.1°$). The FRS angle is sinusoidally modulated through alternating the magnetic field ($\Theta\sin(\omega_m t)$) and the FRS signal is measured by demodulating the associated intensity changes at the 1st harmonic of the modulation signal as schematically shown in Fig. 1(b). With a small signal approximation the measured FRS signal, $S_{C\text{-}FRS}$, is proportional to the first derivative of the analyzer transmission curve in Fig. 1(b), which yields $S_{C\text{-}FRS} \propto d(\sin^2\theta + \xi)/d\theta = \sin(2\theta)$. Since the FRS signal vanishes at $\theta = 0$ the optimum SNR for conventional FRS system occurs at the analyzer angle that is slightly offset from the zero position. It has been shown that at optimal θ the laser noise equals the detector noise, and further uncrossing would deteriorate the SNR.

In contrast to C-FRS the H-FRS employs detection of the wave amplitude (not intensity/power) that is proportional to $\sin\theta$ after the analyzer. If 1st harmonic demodulation is applied, the FRS signal can be approximated as $S_{H\text{-}FRS} \propto \cos\theta$, which at $\theta = 0$ exhibits maximum (Fig. 1(c)). Thus if the laser noise is sufficiently suppressed the $\theta = 0$ is an optimum analyzer position for H-FRS measurements. When FRS angle is sinusoidally modulated at ω_m the field in the ordinary beam transmitted through the analyzer at $\theta = 0$ can be described as:

$$E' = E_0 \Theta \sin(\omega_m t) \tag{2}$$

where $E_0 \propto P_0^{1/2}$ is the optical field amplitude before the analyzer and Θ is the Faraday rotation angle amplitude. Since $\Theta\sin(\omega_m t)$ is usually very small an approximation $\sin(\Theta\sin(\omega_m t)) \sim \Theta\sin(\omega_m t)$ has been applied in Eq. (2). For small θ most of the laser power P_0 is transmitted into extraordinary beam. This beam is directed into an AOM, which is used to frequency-shift the extraordinary wave by Ω. This radiation is then passed through a 90 degrees polarization rotator and serves as the LO with amplitude E_{LO}. The two beams (the signal and the LO beam) are then combined on a beam splitter and focused on a photodetector. A square-law detector serves as a heterodyne mixer, which generates a photocurrent:

$$\begin{aligned} I &\propto (E' + E_{LO})^2 = (E')^2 + E_{LO}^{\ 2} + 2E' \cdot E_{LO} \cdot \cos(\Omega t + \Phi) \\ &\propto P_{LO} + 2\sqrt{P_0 P_{LO}} \cdot \Theta \cdot \sin(\omega_m t) \cdot \cos(\Omega t + \Phi) \end{aligned} \tag{3}$$

Since $(E')^2 << E_{LO}^2$, the DC component of the photocurrent in Eq. (3) comes primarily from P_{LO}. The second term is the H-FRS signal, which has a form of carrier-suppressed amplitude modulation (Fig. 1(d)). The H-FRS signal S that is retrieved through amplitude demodulation of the RF beatnote can be expressed as:

$$S = 2R_V \eta_{het} \frac{\eta e}{h\nu} \sqrt{P_0 P_{LO}} \Theta \tag{4}$$

where R_V is the photodetector transimpedance, $\eta e/h\nu$ is the current responsivity of a photodetector with quantum efficiency η (e and $h\nu$ are the electron charge and a photon energy, respectively), and η_{het} is the heterodyne efficiency. Similarly to C-FRS, there are three main noise contributions: the photodetector noise, the laser-generated shot noise and the laser amplitude noise. Given the LO accounts for most of the detected laser power all three individual noise contributions measured at the photodetector voltage output can be expressed as bandwidth-normalized quantities:

$$N_{PD} = \sqrt{\Delta f} \cdot R_V \cdot \frac{\eta e}{h\nu} \cdot NEP \tag{5}$$

$$N_{shot} = \sqrt{\Delta f} \cdot R_V \cdot \sqrt{2e \cdot \frac{\eta e}{h\nu} \cdot P_{LO}} \tag{6}$$

#177574 - $15.00 USD Received 8 Oct 2012; revised 20 Nov 2012; accepted 21 Dec 2012; published 7 Jan 2013

$$N_{RIN} = \sqrt{\Delta f} \cdot \sigma(\Omega \pm \omega_m) \cdot R_V \cdot \frac{\eta e}{h\nu} P_{LO} \tag{7}$$

where shot noise N_{shot} in Eq. (6) is derived from photocurrent shot noise density $i_{shot} = \sqrt{2eI_{LO}}$ converted to output voltage based on photodetector/preamplifier parameters, and $\sigma(\Omega \pm \omega_m)$ in Eq. (7) denotes laser RIN measured at frequency $\Omega \pm \omega_m$. As mentioned above, the AC component in Eq. (3) has a form of carrier-suppressed amplitude modulation. This is central to the concept of the H-FRS measurement, because with fully suppressed carrier the heterodyne conversion of the large noise in the baseband to high frequencies should not exist and the measured laser noise should only originate from the LO noise at frequency $\Omega \pm \omega_m$ away from the baseband (shown as $\sigma(\Omega \pm \omega_m)$ in Eq. (7). Because in the RF frequency range the 1/f laser noise becomes extremely small, by setting Ω sufficiently high the measured LO noise is strongly suppressed. Therefore with relatively high intensity of LO the shot noise cannot be neglected in the H-FRS, which is rarely the case in conventional FRS systems. In the following section certain conditions at which quantum shot noise limited performance can be achieved are discussed.

2.2. Condition for shot noise limited photodetection

In order to assure shot noise limited photodetection in any optical system the following conditions should be met: a) the laser intensity noise should be smaller than the shot noise ($N_{shot} > N_{RIN}$), and b) the photodetector noise should be smaller than the shot noise ($N_{shot} > N_{PD}$). With an assumption of a general case of photodetection at wavelength λ, with a signal frequency f and demodulation bandwidth Δf this two conditions can be expressed as:

$$\sqrt{\Delta f} \cdot R_V \cdot \sqrt{2e \cdot \frac{\eta e}{h\nu} \cdot P} > \sqrt{\Delta f} \cdot \sigma(\lambda, f) \cdot R_V \cdot \frac{\eta e}{h\nu} \cdot P \tag{8}$$

$$\sqrt{\Delta f} \cdot R_V \cdot \sqrt{2e \cdot \frac{\eta e}{h\nu} \cdot P} > \sqrt{\Delta f} \cdot R_V \cdot \frac{\eta e}{h\nu} \cdot NEP(\lambda, f) \tag{9}$$

If solved for optical power both equations can be simplified to:

$$\sqrt{P_{\min}} = NEP(\lambda, f) \cdot \sqrt{\frac{\eta}{2h\nu}} < \sqrt{P} < \frac{1}{\sigma(\lambda, f)} \sqrt{\frac{2h\nu}{\eta}} = \sqrt{P_{\max}} \tag{10}$$

Equation (10) indicates that generally in a given optical system a shot noise dominated photodetection can be performed within a well-defined range of collected laser power P between P_{min} and P_{max}. If the power collected by the photodetector is smaller than P_{min}, photodetector noise dominates, while if the collected power is larger than P_{max} the system becomes laser noise limited. A more general condition that can be obtained from Eq. (10) is $NEP(\lambda, f)\sqrt{\frac{\eta}{2h\nu}} < \frac{1}{\sigma(\lambda, f)} \sqrt{\frac{2h\nu}{\eta}}$, which after simplification can be expressed as:

$$\sigma(\lambda, f) \cdot NEP(\lambda, f) < \frac{2h\nu}{\eta} \tag{11}$$

Optical systems that do not satisfy this condition are not capable of shot noise dominated performance. Once the laser RIN, detector NEP and detector quantum efficiency are known, Eq. (11) can be used to determine if the shot noise limited performance is feasible with a given detection system. Please note that the optical power is not a factor that determines if the system is able to provide shot noise limited performance. It also indicates that at shorter wavelengths (higher frequencies ν) where diode lasers with lower RIN and photodetectors with lower NEP are available, shot noise limited performance of optical sensing is relatively

#177574 - $15.00 USD Received 8 Oct 2012; revised 20 Nov 2012; accepted 21 Dec 2012; published 7 Jan 2013

easier to achieve [13]. However, as it will be shown later in this paper, although the shot noise limit represents the best performance for a given system, it does not guarantee the smallest noise-equivalent Faraday rotation angle among other FRS systems, because parameters such as optical power and photon energy used in the measurement must also be taken into account.

2.3. Ultimate detection limit for C-FRS and H-FRS

If laser RIN is negligible and there is sufficient optical power on the detector operating below its saturation regime, the general condition in Eq. (11) is met and the total noise becomes dominated by photocurrent shot noise. In such a case Eq. (4) and (6) can be used to calculate the shot noise equivalent detectible polarization rotation angle for H-FRS:

$$\Theta_{SNEA_{H-FRS}} = \sqrt{\Delta f} \cdot \frac{1}{\eta_{het}\sqrt{2}} \cdot \sqrt{\frac{h\nu}{\eta P_0}} \tag{12}$$

The shot noise-equivalent Faraday rotation angle is inversely proportional to the square root of an average photon flux available before the analyzer adjusted by the quantum efficiency of the photodetector. The detection limit is also affected by the heterodyne efficiency which affects the signal and in practice is smaller than unity. In an ideal case with $\eta_{het} = 1$ this result is consistent with the phase sensitivity of a shot noise limited Michelson interferometer [34]. This confirms that FRS is actually a sensitive phase (dispersion) measurement and not an amplitude (absorption) measurement.

Similarly the shot noise-equivalent Faraday rotation angle can be calculated for a conventional FRS based on 90-degree method [33] yielding:

$$\Theta_{SNEA_{C-FRS}} = \frac{\sqrt{\Delta f} \cdot R_V \cdot \sqrt{2e \cdot \frac{\eta e}{h\nu} \cdot P_0 \sin^2\theta}}{R_V \cdot \frac{\eta e}{h\nu} \cdot P_0 \sin(2\theta)} = \sqrt{\Delta f} \cdot \sqrt{\frac{2h\nu}{\eta P_0}} \cdot \frac{\sin\theta}{\sin(2\theta)} \tag{13}$$

For $\theta << 1$, which is true for most 90-degree FRS systems the last factor in the equation can be approximated as $\sin\theta/\sin(2\theta) \sim 1/2$ and Eq. (13) becomes identical with Eq. (12) (if $\eta_{het} = 1$ is assumed). Therefore in theory, both H-FRS and C-FRS can reach the same ultimate sensitivity when operated in shot noise limited regime. In this regime the sensitivity to the sample can only be enhanced by improving the optical power P_0 or by increasing the optical path within the sample to enhance the FRS rotation angle (please note that by applying a multi-pass arrangement to increase the interaction path the optical power P_0 will be also affected, which must be taken into account in sensitivity estimations [35]). It should also be noted that at shorter wavelengths/higher frequencies (given all other parameters are the same) the ultimate detection limit of FRS systems becomes gradually decreased.

3. Experimental setup

A schematic diagram of the H-FRS experimental setup is shown in Fig. 2. The laser source is a 5.24 μm continuous wave DFB QCL (provided by Alpes Lasers SA), operating near room temperature. The QCL temperature is stabilized using a TEC with a temperature controller (Arroyo Instruments 5305) and the bias current is delivered from a low noise current driver (Wavelength Electronics QCL500). The laser beam is collimated with a ZnSe lens (f = 1.9 mm) and directed through the first polarizer (RP1) that is used to improve the polarization quality and to precisely set the polarization axis of the light incident on the sample. RP1 is followed by a 15 cm gas cell surrounded by an electromagnetic solenoid driven with a power amplifier (RMX 850). By supplying current of 3 A (root-mean-square, rms) to the solenoid, an axial magnetic field of 100 G_{rms} (Gauss-rms) modulated at frequency $f_m = 1.08$ kHz was obtained within the sample volume. The magnetic field strength in the FRS cell was carefully characterized with a Gauss-meter. The 100 G_{rms} was an average value estimated for the active

#177574 - $15.00 USD Received 8 Oct 2012; revised 20 Nov 2012; accepted 21 Dec 2012; published 7 Jan 2013

optical path inside the gas cell (the field is non-uniform along the optical axis with stronger field at the center and ~50% weaker at both ends of the cell).

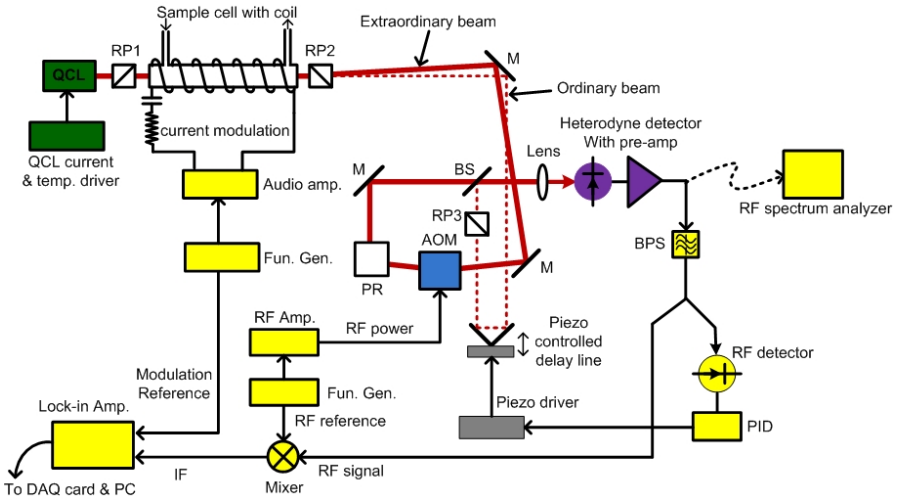

Fig. 2. Schematic diagram of the H-FRS setup. BS: 50/50 beam splitter; M: mirror; AOM: acousto-optical modulator; PR: polarization rotator; RP: Rochon polarizer; Fun. Gen.: function generator; BPS: band pass filter centered at 30 MHz with a bandwidth of 6 MHz.

When the laser optical frequency coincides with the target NO transition, the linearly polarized light undergoes Faraday rotation. The analyzer RP2 placed after the gas cell (Rochon prism with an extinction ratio of ~1×10^{-5}) transforms polarization rotation into the wave amplitude modulation as described by Eq. (2). The polarization axis of the ordinary beam emerging from Rochon analyzer is fully crossed ($\theta = 0°$) with respect to the RP1 which guarantees maximum H-FRS signal. When there is no Faraday rotation, only a small fraction of the laser power determined by the effective extinction ratio leaks through the analyzer. The effective extinction ratio of the system that consists of the RP1, the gas cell, and the RP2, was measured to be ~1.86×10^{-4}. This is higher value than the Rochon prism specification, and we attribute it to the deterioration of the polarization quality by the cell windows. Therefore a third polarizer RP3 set to the same polarization as RP2 was placed within the ordinary beam path, which allowed for an additional factor of 5 improvement in the effective polarization extinction ratio. The extraordinary beam emerging from Rochon analyzer undergoes a frequency shift by $\Omega = 30$ MHz with an AOM (IntraAction AGM-40) and then serves as the LO. The AOM is driven by a low noise function generator (Tektronix AFG 3102) and RF power amplifier (HP 230B) that provide more than 80 dB phase noise suppression ratio at ~1 kHz. Temperature stabilized water cooling (SolidState Cooling ThermoRack 650) is applied to the AOM in order to minimize refractive index variations caused by thermal drifts. Since the heterodyne efficiency is sensitive to the polarization of the two waves, the extraordinary beam is directed through a periscope assembly (Thorlabs RS99) used to perform a simple 90° rotation of the polarization axis [36]. The two beams (signal and LO) are then re-combined using a calcium fluoride beam splitter (BS) with 50/50 split ratio and then are focused by an aspheric ZnSe lens (Thorlabs AL72512-E) onto a TEC-cooled MCT photodetector (VIGO PV-2TE-5 with active area of ~0.05×0.05 mm^2 and dual stage preamplifier unit customized for heterodyne detection). The photodetector has cut-off frequency of 59 MHz, a relatively low NEP of ~1×10^{-11} W/Hz$^{1/2}$, and a saturation optical power of 1.2 mW. A band pass filter (BPS) with 6 MHz bandwidth centered at 30 MHz is used for signal filtering and rejection of large noise at low frequencies. A double balanced frequency mixer (Mini-circuits ZX051LS +) is used to down-covert the RF heterodyne signal at 30 MHz to the base band (IF output in Fig. 2) by mixing it with a reference signal from the function generator. The IF output of the

#177574 - $15.00 USD Received 8 Oct 2012; revised 20 Nov 2012; accepted 21 Dec 2012; published 7 Jan 2013

mixer is demodulated by a lock-in amplifier (Signal Recovery 7265) at the magnetic field modulation frequency f_m to retrieve the FRS signal. The FRS signal is then recorded by a PC equipped with a data acquisition card (NI USB-6251).

The QCL is operated in a wavelength-scan mode performed by slow variation of the laser injection current to acquire an FRS spectrum around the target transition R(17/2) at 1906.73 cm^{-1}. To test the system performance a calibrated gas mixture containing 2 ppmv (parts per million by volume) of NO balanced with dry N_2 is flown through the gas cell. The pressure in the gas cell is stabilized at 30 Torr by a pressure controller (MKS πPC PC99).

Due to unpredictable temperature drifts of the AOM (that affect optical phase in the interferometer's LO arm) strong changes in the measured heterodyne signal phase have been observed. Ideally, when the path lengths of the ordinary beam and the extraordinary LO beam are perfectly balanced, a wavelength dependent phase drift of the heterodyne signal will be eliminated. In order to keep those two paths equal in length, an actively controlled optical delay line is incorporated into ordinary beam path. A total observed RF power of the heterodyne beatnote is used to derive an error signal and to perform active control of the optical delay line. This is possible because the LO beam carries a small portion of residual amplitude modulation (RAM) at frequency Ω introduced by the AOM, and its phase does not change with the interferometer drift. However the superposition of the phase-stable RAM and a phase-drifting heterodyne signal (both at 30 MHz frequency) results in a varying power of the RF carrier at 30 MHz which is then used as a feedback signal for interferometer stabilization. The active path length control is implemented as shown in Fig. 2. A piezoelectric actuator with 10 nm resolution (Thorlabs PE4) and a PID controller (SRS SIM960) are used to control the optical delay line and to stabilize the path length. The error signal for the feedback loop is derived from portion of the photodetector output power measured by a high sensitivity Schottky diode (Herotek DHM020BB) compared to a constant set point. Despite introducing additional complication into the optical system this active feedback method has an advantage of being able to perform the H-FRS measurement with only one photodetector element. This complication could be avoided if a balanced heterodyne receiver is used to measure both outputs of the interferometer. However, similarly to conventional balanced photodetectors discussed earlier, there is no mid-IR balanced heterodyne photoreceivers available commercially and custom devices can be costly. Therefore the single photodetector approach implemented here is more viable at this time.

4. Results and discussion

4.1. Noise analysis

The system noise spectrum in the range between 10 kHz and 100 MHz was recorded directly at the output of the photodetector using an RF spectrum analyzer (Tektronix RSA6106A) and the results are shown in Fig. 3. The photodetector noise was measured with the laser light blocked and is shown as a black line in Fig. 3. The red trace shows the total noise measured with the QCL light incident on the detector. During this measurement, the laser driving current was kept at 160 mA, the laser temperature was 0°C, and the power on the detector was set to 120 μW. At such a low power level the shot noise is lower than photodetector noise. Therefore, the increase in the noise level observed between the black and red traces shown in Fig. 3 indicate primarily an influence of the laser noise. As expected in the low frequency range the laser noise generally follows 1/f trend, and at frequencies >1MHz there are some distinct peaks that can be avoided by selecting an appropriate measurement frequency. We have not studied the origin of those distinct peaks in the noise spectrum between 1 MHz and 10 MHz, but we suspect the noise of the laser current source, power supplies, and TEC controller electromagnetic interference are the most possible causes of this specific spectral noise structure. Generally the noise floor at higher frequencies (> 500kHz), is much lower than the noise level at 10 kHz. We found that in the present system the frequency of 30 MHz

#177574 - $15.00 USD Received 8 Oct 2012; revised 20 Nov 2012; accepted 21 Dec 2012; published 7 Jan 2013

is optimal for heterodyne detection (as shown in Fig. 3 inset). At 30 MHz, both the photodetector and the laser noise are strongly reduced while the detector is still fast enough to detect signals (it operates well below its 3dB cut-off frequency). An AOM designed for frequency range between 30 MHz and 50 MHz was used to produce the LO.

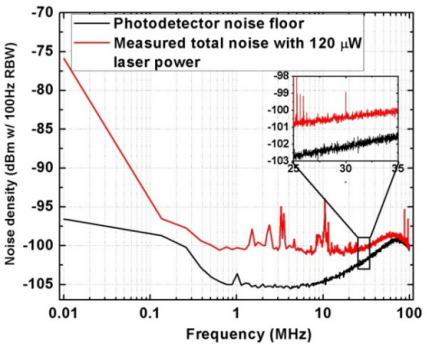

Fig. 3. Noise spectrum recorded at the detector output without (black) and with the laser light shining at the detector (red). The contribution of the laser noise is clearly noticeable. The resolution bandwidth (RBW) of the RF spectrum analyzer is 100 Hz. QCL was operated at 0°C with 160 mA bias current, and the optical power on the photodetector was set to ~120 μW.

In order to compare how far from the fundamental shot noise limit both the C-FRS and the H-FRS would operate in this setup, the noise contributions relevant in both configurations were carefully characterized. The noise for C-FRS has been evaluated at the coil modulation frequency f_m = 1.08 kHz and for H-FRS the noise at Ω was taken into account. Because the available RF analyzer cannot measure signals below 9 kHz, the noise characterization at f_m = 1.08 kHz was performed using a lock-in amplifier. In both cases the noise measurement was performed as a function of optical power. A constant laser current of 160 mA was used in both measurements and the optical power on the photodetector was varied by rotating a polarizer placed between laser and detector. The C-FRS noise measurement results are shown in Fig. 4(a). The RIN analysis is performed using noise data that are far above the photodetector noise and the shot noise. The slope of a linear fit to the noise data as a function of optical power level shown in Fig. 4(a) represents the laser RIN of $\sigma(\omega_m) = 2.94 \times 10^{-6}$ $Hz^{-1/2}$.

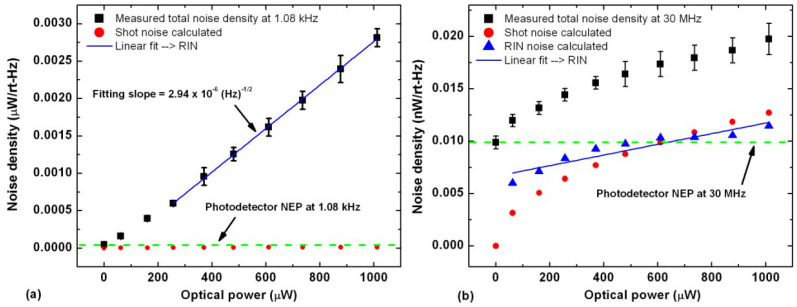

Fig. 4. (a) The photodetected noise density at 1.08 kHz (black dots) as a function of laser power. A slope of a linear fit (blue line) to the data in laser noise dominated regime is used to measure RIN. For comparison, shot noise calculated from Eq. (6) is shown by red dots. The QCL is operated at 160 mA, and at heatsink temperature of 0°C. Optical power was adjusted by the polarizer. Green dash line indicates the measured photodetector noise, which corresponds to NEP = 4.8×10^{-11} $W/Hz^{1/2}$ at 1.08 kHz. (b) The total noise (black dots) at ~30 MHz measured with an RF spectrum analyzer as a function of optical power. The same QCL operating conditions were used as in Fig. 4(a). The shot noise (red dots) and laser noise (blue dots) were calculated based on photodetector current responsivity of 2.0 A/W, and detector transimpedance of 8350 V/A. The green dashed line indicates the measured photodetector noise, which at ~30 MHz corresponds to NEP = 1×10^{-11} $W/Hz^{1/2}$.

#177574 - $15.00 USD Received 8 Oct 2012; revised 20 Nov 2012; accepted 21 Dec 2012; published 7 Jan 2013

For comparison, Fig. 4(b) shows the noise vs. optical power characteristics for the same laser operating conditions as in Fig. 4(a), but measured at Ω = (30 MHz + 1.08 kHz) using RF spectrum analyzer. It is clear that the shot noise calculated from Eq. (6) is not negligible at this frequency. The laser noise $N_{RIN} = P \cdot \sigma(\Omega)$ (blue triangles in Fig. 4(b)) is calculated as:

$$N_{RIN} = \sqrt{N_{total}^2 - N_{shot}^2 - N_{PD}^2} \tag{14}$$

where the N_{total} is the total noise (measured), N_{PD} is the detector noise (measured), and the N_{shot} is the shot noise (calculated). As shown in Fig. 4(b), the laser noise at ~30 MHz is almost at the same level as the shot noise. The calculated RIN of $\sigma(\Omega) = 7.98 \times 10^{-9}$ $Hz^{-1/2}$ is ~370 times lower than the RIN measured at 1.08 kHz. The H-FRS enables performing shot noise dominated measurements in a system which at low frequencies is dominated by laser noise. With a photodetector NEP of 1.0×10^{-11} $W/Hz^{1/2}$ (measured at 30 MHz) Eq. (10) gives a range of LO power of 0.66 mW<P_{LO}<2.39 mW, within which shot noise limit can be reached. This is in excellent agreement with the data in Fig. 4(b), which clearly show that for optical powers above 0.66 mW the shot noise becomes higher than the photodetector noise. For optical power of ~1 mW, the total noise is only 1.56 times higher than the shot noise. The high power limit could not be verified, because the photodetector preamplifier saturates for optical powers above 1mW.

4.2. Signal-to-noise ratio

Heterodyne efficiency η_{het} is one of the factors that affect the signal strength and thus the detection limit in H-FRS. In the theoretical analysis above we have assumed $\eta_{het} = 1$, which requires the interfering signal and LO waves to be perfect plane waves with exactly the same polarization state and ideally aligned wavefronts at the photodetector plane. However in practice there are multiple factors such as wavefront quality distortions, polarization-degradation, imperfect mode matching, or photodetector nonlinearity that can reduce the heterodyne efficiency. In the H-FRS system discussed here the heterodyne efficiency was evaluated experimentally using fixed LO power at 60 μW and several values of signal beam power varied between 10 and 70 μW. The average heterodyne efficiency measured in our system was $\eta_{het} = 0.5$ (the photodetector quantum efficiency has been accounted for in the calculation). This is a reasonable value given many transmissive components that potentially can deteriorate wavefront and polarization quality in this H-FRS system prototype.

Figure 5 shows a typical H-FRS spectrum acquired with the system. The QCL wavelength was scanned across the NO R(17/2) transition by stepping the bias current of the QCL from 160 mA to 163 mA with 0.017 mA steps. The laser frequency tuning rate was approximately ~0.033 cm^{-1}/mA. The LO power on the photodetector was set to the maximum value of ~1 mW permitted by the photodetector specifications. The lock-in amplifier time constant was set to 200 ms (with 12dB/octave filter slope) which gives effective detection bandwidth of Δf = 0.83 Hz. We have identified that the asymmetry in the measured spectrum was caused by the combination of MCB and MCD effects similarly to references [10, 37]. Contribution of the MCD signal can be suppressed when analyzer offset angle is set very precisely at 0°. In the present system a manual adjustment of the polarization axis did not provide sufficient precision to eliminate the MCD contribution below detectible level. In future works, a motorized rotary stage with resolution of 0.001° will be used to increase the adjustment accuracy and to automatize the process of suppressing the MCD effects in the acquired spectra. However the peak of the H-FRS spectrum is not affected by the presence of the MCD contribution (which has derivative-like shape with a zero-crossing at the line center). This allows for reliable and reproducible estimation of the system's SNR by using the signal amplitude at the line center and the noise measured as a standard deviation of the spectral data points away from the transition. Based on data in Fig. 5, the signal strength at the peak is S = 76.8 μV (measured with respect to the baseline offset) and the noise spectral density of N =

#177574 - $15.00 USD Received 8 Oct 2012; revised 20 Nov 2012; accepted 21 Dec 2012; published 7 Jan 2013

0.792 ± 0.066 μV/Hz$^{1/2}$ has been measured. This corresponds to an SNR of ~105, which yields a bandwidth-normalized NO concentration detection limit of 20.6 ppbv/Hz$^{1/2}$.

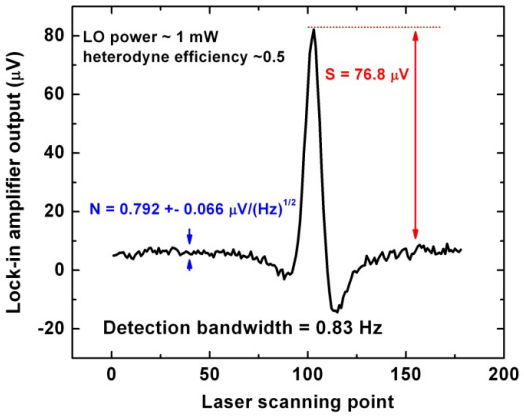

Fig. 5. An H-FRS spectrum of the NO R(17/2) transition at 1906.73 cm^{-1}. Experimental conditions: 2 ppmv NO in N_2 mixture, sample pressure of 30 Torr, sample temperature of 300 K, magnetic field of ~100 G, active optical pathlength L = 15 cm, optical power before analyzer P_0 = 14 mW, LO power P_{LO} = 1 mW, photodetector current responsivity 2.0 A/W, transimpedance R_v = 8350 V/A, heterodyne efficiency η_{het} = 0.5, and a measurement bandwidth of 0.83 Hz. The system electrical gains have been factored in and the y-scale reflects voltage at the detector output.

The measured noise spectral density is approximately 2.4 times larger than the total noise observed for this system with RF spectrum analyzer in Fig. 4(b) and 3.7 times larger than the fundamental shot-noise level calculated for P_{LO} = 1mW. This slight deterioration with respect to Fig. 4(b) was expected because the frequency mixer used in the H-FRS system contributes additional noise (the noise figure specified by the manufacturer is ~5.6 dB), as well as the system was found to be sensitive to mechanical vibrations that also contribute noise that cannot be corrected by the relatively slow active stabilization of the interferometer implemented in this system. Despite this small increase in the total system noise an excellent noise equivalent Faraday rotation angle of $\Theta_{NEA}/\Delta f^{1/2} = 1.79 \times 10^{-8}$ rad/Hz$^{1/2}$ has been obtained (the value is estimated by equating the measured noise N to the signal S in Eq. (4) reduced by factor of $2^{1/2}$ to account for signal amplitude loss on the 50/50 beam splitter). When compared to the ultimate shot noise equivalent Faraday rotation angle of 3.2×10^{-9} rad/Hz$^{1/2}$ calculated for this system using Eq. (12), the experimental result is only about factor of 5.6 times worse (which agrees with the signal loss at the beam splitter by $2^{1/2}$ times and with the noise that is 3.7 times higher than the calculated shot noise level).

4.3. Comparison with other FRS systems

For comparison with other FRS results we have surveyed experimental results obtained with cryogen-free FRS systems published recently. The three experimental setups published in Refs [6], [7], and [13] show different sources of performance limitations.

In the NO sensing system reported in Ref [6], the noise equivalent Faraday rotation angle measured with a TEC cooled detector was 2.53×10^{-7} rad/Hz$^{1/2}$ (calculated as rms value for the experimental conditions used in this work). The system uses the $Q_{3/2}(3/2)$ transition that is optimum for FRS measurements of NO at low magnetic fields. This transition exhibits the highest g-factor that allows to produce optimum Zeeman splitting (on the order of absorption line width) with relatively low magnetic field (~100-200 G) [4–6]. The minimum detectible polarization rotation in this system corresponds to NO detection limit of 3.8 ppbv-m/Hz$^{1/2}$ (the detection limit is normalized to optical path and measurement bandwidth of Δf = 0.25Hz estimated for 1 s time constant and 6dB/octave filter slope). However the fundamental shot

#177574 - $15.00 USD Received 8 Oct 2012; revised 20 Nov 2012; accepted 21 Dec 2012; published 7 Jan 2013

noise limit of 3.62×10^{-9} rad/Hz$^{1/2}$ calculated for the system parameters using Eq. (13) is ~70 times better, which indicates that system is strongly dominated by laser/detector noise. Therefore after application of a liquid nitrogen cooled InSb detector in this work an improvement in the detection limit by factor of 11.3 was achieved. The overall performance of the system with cryogenically cooled detector corresponds to ~6.2 times the shot noise limited performance.

Kluczynski *et al.* in Ref [7] used a DFB QCL to target the same $Q_{3/2}(3/2)$ transition of NO and a single spectral point NO detection limit of 1.03 ppbv-m/Hz$^{1/2}$ (also path- and banwidth-normalized) was obtained. A spectroscopic modeling performed for the reported detection limit achieved with 15 cm optical path, sample gas pressure of 67 mbar (~50 Torr), and magnetic field of 156 G (rms) yields the noise equivalent Faraday rotation angle of 7.89×10^{-8} rad/ Hz$^{1/2}$, which is two orders (~99) of magnitude worse than the ultimate shot noise limited performance of 7.96×10^{-10} rad/ Hz$^{1/2}$ estimated for the available laser power of 60 mW. This suggests that the laser noise was still the primary limiting factor in Ref [7]. Theoretically, if the laser RIN was comparable in both experiments, a 20-fold increase in optical power and 0.72 times lower NEP in Ref [7] should improve the $\Theta_{NEA_{C-FRS}}$ by approximately 5.3 times ($(20/0.72)^{1/2}$) with respect to Ref [6]. Since there is only ~3 × improvement in minimum detectible rotation angle, this indicates 3 times higher laser RIN in Ref [7] as compared to the laser used in Ref [6]. In conclusion both NO systems could tremendously benefit from a reduction of their laser noise below the fundamental shot noise limit with a prospect of up to two orders of magnitude improvement in sensitivity.

A conventional FRS system with shot noise dominated performance was reported by Zhao *et al.* [13]. In this setup targeting detection of OH-radicals the measured minimum detectible Faraday rotation angle of 1.39×10^{-7} rad/Hz$^{1/2}$ was only 2.1 times higher than the theoretical shot noise limit of 6.62×10^{-8} rad/Hz$^{1/2}$. By analyzing the fundamental limit provided in Eq. (12) one can clearly see that the detection performance of the OH system was impeded by relatively low optical power (15μW) and by the higher energy of the photon at 2.8μm. This yields >10 times worse ultimate detection limit as compared to NO sensing systems operated at 5.3 μm. Therefore despite close to shot-noise limited performance the actual noise equivalent Faraday rotation angle achievable by this system was very similar to the results obtained with the other two conventional FRS systems discussed above.

The performance of the H-FRS described in this paper can now be directly compared to the three conventional FRS systems mentioned above. Table 1 shows a summary of parameters for all FRS systems discussed (including a separate column for the system from Ref [6] based on cryogenically cooled detector).

In terms of the ultimate shot-noise limited sensitivity all NO sensing systems were very similar (within factor of 5 between the highest and the lowest limit) and the OH system shows the lowest performance limit due to the reasons described above. In terms of the actual noise equivalent Faraday rotation angle the H-FRS system outperforms all C-FRS systems by: a) a factor of 14 with respect to Ref [6], b) a factor of 1.3 with respect to system with cryo-cooling in Ref [6], c) a factor of 4.4 with respect to Ref [7] and d) a factor of 7.8 with respect to Ref [13]. Most importantly the H-FRS system approaches the shot noise limited operation (with a noise floor of 3.7 times the shot noise) by utilizing the heterodyne process and a non-cryogenically cooled detector. This is obtained through recycling of the optical power that is normally lost in 90-degree FRS systems and using it as a LO in the H-FRS measurement. It is obvious that despite significant improvement in terms of the noise equivalent Faraday rotation angle the sensitivity to NO concentration for the H-FRS system is up to 3 times lower than for cryogen-free C-FRS systems referenced above. The higher concentration sensitivity of the two C-FRS sensors is determined primarily by the target NO transition that is optimal for FRS measurements at low magnetic fields. Although the NO $Q_{3/2}(3/2)$ transition at 1875.8cm^{-1} has 1.4 lower absorption line intensity than the R(17/2) transition at 1906.73 cm^{1}, a significantly

#177574 - $15.00 USD Received 8 Oct 2012; revised 20 Nov 2012; accepted 21 Dec 2012; published 7 Jan 2013

higher g-factor in the Q-branch (see Table 1) allows for more optimal Zeeman split at relatively low magnetic field (~100 G_{rms}). The R(17/2) shows approximately 15 times lower magnetic modulation sensitivity than $Q_{3/2}(3/2)$ (this was estimated by adding magnetic modulation sensitivities of all allowed transitions [4]). A simulation of the FRS spectrum for our experimental conditions yields FRS signal for the $Q_{3/2}(3/2)$ transition that is ~6 times stronger than for the R(17/2) transition targeted in this work. After accounting for this straight forward signal enhancement the cryogen-free H-FRS system equipped with a laser targeting $Q_{3/2}(3/2)$ transition is expected to achieve concentration sensitivity of 0.5 ppbvm/$Hz^{1/2}$. Such a performance would be comparable to the C-FRS system based on LN_2 cooled InSb detector in Ref [6] but without the need for cryogenic cooling (see Table 1 for details).

Table 1. Performance comparison of selected conventional FRS systems with H-FRS.

	C-FRS with TEC MCT detector [6]	C-FRS with LN_2 cooled InSb detector [6]	C-FRS [7]	C-FRS [13]	H-FRS
$\Theta_{SNEA}/(\Delta f)^{1/2}$* Theoretical limit [rad/$Hz^{1/2}$]	3.62×10^{-9}	3.62×10^{-9}	7.96×10^{-10}	6.62×10^{-8}	3.2×10^{-9}
$\Theta_{NEA}/(\Delta f)^{1/2}$ Measured [rad/$Hz^{1/2}$]	2.53×10^{-7}	2.24×10^{-8}	7.89×10^{-8}	1.39×10^{-7}	1.79×10^{-8}
$\Theta_{NEA}/\Theta_{SNEA}$	70	6.2	99	2.1	5.6
Molecule	NO	NO	NO	OH	NO
Target transition	$Q_{3/2}(3/2)$	$Q_{3/2}(3/2)$	$Q_{3/2}(3/2)$	Q(3/2)	R(17/2)
Line intensity (cumulative for all transitions) [cm/molecule]	3.16×10^{-20}	3.16×10^{-20}	3.16×10^{-20}	9.45×10^{-20}	4.5×10^{-20}
Frequency [cm^{-1}]	1875.8	1875.8	1875.8	3568.5	1906.73
g′/g″ **	0.78/0.78	0.78/0.78	0.78/0.78	0.93/0.93	0.0026/0.0096
Detection limit (path- and bandwidth-normalized) [ppbv-m/$Hz^{1/2}$]	3.78	0.334	1.03	8.88	3.09 (~0.5***)
Primary sensitivity limiting factors	Laser RIN, photodetector NEP	Laser RIN	Laser RIN	Low laser power, high photon energy	Non-optimum spectral line; Signal loss due to beam splitter; low heterodyne efficiency; RF mixer noise

*Note: the shot noise $\Theta_{SNEA}/(\Delta f)^{1/2}$ is calculated with Eqs. (12) and (13) based on the actual experimental conditions: P_0 = 2.9 mW for Ref [6], P_0 = 60 mW for Ref [7], P_0 = 0.015 mW for Ref [13], and P_0 = 14 mW was used for H-FRS. The detector quantum efficiency of $\eta = 0.5$ was assumed in all C-FRS systems, which is a moderate number that should provide a good approximation of the system's fundamental limit. A measured $\eta_{het} = 0.5$ was used for H-FRS.
**Note: g-factors for the upper state (*g′*) and the lower state (*g″*) respectively.
***Note: Detection limit estimated for $Q_{3/2}(3/2)$ transition of NO at 1875.8cm^{-1}.

5. Conclusions

A heterodyne enhanced Faraday rotation spectroscopy has been introduced. When compared to a conventional FRS, the H-FRS offers several advantages that improve system performance and allow close-to fundamental noise limited operation. Especially when combined with mid-IR QCL sources, which show significant laser noise in the low frequency region (DC to ~100 kHz), the shift of FRS detection to the RF frequencies enables near shot noise limited performance of the system. In our system the laser RIN at 30MHz used for H-FRS is ~370 times lower than that observed at the f_m of 1.08 kHz for C-FRS. Moreover, theoretically the H-FRS can suppress electromagnetic interference (EMI) caused by the high AC currents used

#177574 - $15.00 USD Received 8 Oct 2012; revised 20 Nov 2012; accepted 21 Dec 2012; published 7 Jan 2013

to generate modulated magnetic fields. Those, if not appropriately shielded, affect the performance of the conventional FRS systems by creating uncontrolled pick-up at the modulation frequency f_m in various parts of the system electronics. Since the signal demodulation in C-FRS is performed at the same frequency, this uncontrolled pick-up becomes a significant issue. In H-FRS system FRS signal is encoded in the heterodyne beatnote at RF frequency Ω, which is significantly higher than f_m and noise at low frequencies (including the pick-up) can be effectively avoided and suppressed by high-pass filters. Therefore, as shown in Fig. 5, H-FRS signal shows significantly lower parasitic offset compared to common 90-degree C-FRS systems (the small offset in Fig. 5 was caused by an insufficient EMI shielding of the electrical components located after the frequency mixer or within the laser driver itself that creates small residual intensity modulation).

An experimental demonstration of H-FRS was performed using a cryogen-free system based on 5.24 μm DFB QCL targeting nitric oxide as the test molecule and a TEC-cooled MCT photodetector. The optical bench-top prototype H-FRS system exhibited the total noise of only 3.7 times (5.7 dB) higher than the quantum shot noise. The noise equivalent Faraday rotation angle of 1.79×10^{-8} rad/Hz$^{1/2}$ is to our knowledge, the best performance achieved among cryogen-free mid-IR FRS systems to date. When the R(17/2) transition of NO at 1906.73 cm^{-1} is used as the target line with 15cm optical path and magnetic field of 100 G_{rms}, this noise equivalent Faraday rotation angle translates to the NO detection sensitivity (1σ) of 20.6 ppbv/Hz$^{1/2}$. The performance of this system can be further improved by optimizing the optical design of the system (e.g. 95/5 beam splitter can be implemented to preserve optical power in the signal beam; a balanced heterodyne receiver can be applied etc.), or a six-fold improvement can be simply achieved by targeting the optimum $Q_{3/2}(3/2)$ transition of NO at 5.33μm. Future optimization of the system towards the shot noise dominated performance should focus on an increase in the heterodyne efficiency, application of more powerful lasers, reduction of a parasitic carrier noise and application of a frequency mixer with lower noise figure.

Acknowledgments

The authors would like to acknowledge the financial support by the National Institute of Health grant #1R21RR026231. Dr. Antoine Muller at Alpes Lasers SA is acknowledged for providing a laser for this study.

#177574 - $15.00 USD Received 8 Oct 2012; revised 20 Nov 2012; accepted 21 Dec 2012; published 7 Jan 2013